# Stand-Still Self-Identification of Flux Characteristics for Synchronous Reluctance Machines Using Novel Saturation Approximating Function and

# Stand-Still Self Identification of Flux Characteristics for SynRM Using Novel Saturation Approximating Function and Multiple Linear Regression

Nicola BEDETTI
Drive and Motion Control Unit
Gefran, s.p.a.
Gerenzano, Varese (Italy)
nicola.bedetti@gefran.com

Sandro CALLIGARO, Roberto PETRELLA
Polytechnic Department of Engineering and Architecture
University of Udine
Udine, Italy
sandro.calligaro@uniud.it, roberto.petrella@uniud.it

***Abstract*—Motor characterization has a fundamental role in dynamics, torque accuracy and efficiency of vector controlled Synchronous Reluctance Motor (SynRM) drives. Control performances and robustness in the whole speed/torque range, including the flux-weakening region, and in sensorless operation strongly rely on the knowledge of machine flux vs. current characteristics. A convenient flux saturation approximating function is proposed in this paper, together with an efficient parameters self-identification procedure. The adopted strategy is very simple and can be performed at standstill by injecting a proper voltage stimulus (current control is not involved), and does not require any additional hardware (motor can be either connected or disconnected from mechanical load). Nevertheless an excellent fitting for the flux curves on both axes is obtained, using reasonable memory and computational resources. These features make the technique very suitable to motor self-identification in industrial drives. Experimental results based on a commercial drive and two SynRM machines are reported to demonstrate the effectiveness of the proposal. Extensions of the method to the evaluation of the whole flux map (including cross-saturation effects) or to interior permanent magnet machines is also investigated and verified.**

***Keywords—Synchronous reluctance machine; synchronous reluctance motor drives; SynRM; magnetic model identification; saturationa; cross-saturation;***

## I. INTRODUCTION

Synchronous Reluctance Machines (SynRM) have been widely investigated since late 1970s, [1]-[4]. However, their adoption is increasingly gaining attention in the last years due to a number of interesting characteristics, e.g. simple and rugged construction, "cold" rotor, short time over load capability, fast dynamic response, wide speed range, deep flux-weakening operations and absence of (costly) permanent magnets. Higher efficiency and lower price may be in fact achieved compared to the induction machine and to permanent magnet synchronous machine respectively, making SynRM attractive for a number of industrial and traction applications, [5]-[8].

Control performances and robustness in the whole speed/torque range, including the flux-weakening region, and in sensorless operation strongly rely on the knowledge of machine parameters, mainly stator resistance and flux vs. current characteristics, [9][10]. Saturation (at least) and cross saturation effects cannot in fact be neglected and complete flux vs. current maps (or inductances) may need to be considered, [11]-[13]. Unfortunately, in many industrial and general-purpose applications, only nameplate motor parameters are available, so a self-commissioning identification procedure needs to be introduced.

Conventional and recently proposed characterization procedures involve time consuming tests to be performed during rotation at constant speed and load [14][15], which often cannot be applied when the drive is already installed, and need to be performed within a laboratory setup. Known techniques, such as no-load identification under acceleration tests, [16], or at stand still with large signal high frequency injection and piecewise linear approximation of the flux curves, [17], may not be suitable in some cases due to mechanical reasons (e.g. motor shaft cannot be decoupled from load) or accuracy issues. In fact, in certain cases, a current bias needs to be applied, [18], which may not be applied to low inertia systems, where it can cause rotation. Moreover, these techniques require at least a current control to be tuned for sufficiently high bandwidth, which in turn involves the knowledge of motor parameters that are going to be estimated.

In this paper a convenient flux saturation approximating function is introduced, which uses only three parameters to characterize the curve. An effective parameters self-identification procedure is proposed, which is very simple to implement. The related tests are performed at standstill by injecting a proper voltage stimulus which must satisfy some simple requirements, on each of the two axes separately. In this way, no torque is produced by the SynRM if axes alignment is accurate, while possible misalignment, until small, only causes high frequency torque components. Current control is not involved in the estimation process, meaning that prior tuning of the current regulators is not required. Despite the simplicity of the method, an excellent fitting for the flux curves on both axes is obtained, using reasonable memory and computational resources. Online use of the obtained characteristics is also relatively low resource consuming.

Experimental identification tests are reported for two different SynRM and for an IPMSM, showing very good agreement with the data obtained from rotational characterization. It is worth noticing that implementation has been carried out using the hardware of a standard commercial

978-1-4673-7151-3/15/$31.00 ©2015 IEEE

drive, demonstrating the feasibility of the method without any need for special hardware (such as a high-speed processor) or particular resources (e.g. oversampling or large memory usage).

Although the method is intended for the identification of SynRM flux maps, results demonstrate that in practice it can be applied to permanent magnet machines as well. However, in this case, apart from the obvious limitation that permanent magnet flux-linkage cannot be identified (no-load rotational tests could be applied instead), the other main issue is that torque is generated during the $q$-axis test. Depending on various factors, including mechanical load characteristics, torque can result in sensible rotor movement, which can cause identification inaccuracy, especially in the case rotor position is not available (sensorless drive). This case will be addressed and results regarding an IPMSM will be reported, showing a very good agreement with the reference measurements.

Finally, the possibility to extend the identification range to the whole $dq$ current range of the machine will be studied. The presented results demonstrate the feasibility of such a technique, although accuracy improvement and some implementation issues still require further investigations.

## II. Novel Flux Saturation Approximating Function

A typical curve that can be adopted to model the saturated flux vs. current characteristics is shown in Fig. 1 (symmetrical behavior is considered for the negative region). At low current levels, flux is approximated to be linear with slope $L_0$, while above a certain positive threshold value $I_{thr}$ a saturating function (linear + inversely proportional) is considered:

$$\begin{aligned} \lambda &= L_0 I \ \text{ for } \ |I| \le I_{thr} \\ \lambda &= sign(I)\ \lambda_0 + L_1 I + \frac{\beta}{I} for\ |I| > I_{thr} \end{aligned} \tag{1}$$

where $I$ is the independent variable (current) and $\lambda$ is the ordinate (flux), while $\lambda_0$, $L_1$ and $\beta$ are constant weight coefficients. In the low current range, i.e. for $|I| \le I_{thr}$, the flux vs. current relation is characterized by the non-saturated inductance $L_0$. In the complementary "high-current" range, if the straight-line asymptote of the curve is considered, the parameters $\lambda_0$ and $L_1$ will be the slope and intercept, respectively. In particular, $L_1$ represents the saturated differential inductance. The positive threshold current value $I_{thr}$ can be thought as an approximation of the knee point of saturation. The value of $\beta$ affects the smoothness of the transition from linear to saturated range: a null value leads to a piecewise linear curve, while negative values result in smoother curves. This model, with appropriate values of the parameters, results in a curve similar to the typical ones describing magnetic saturation, [12], and shows some interesting advantages over other suitable approximating functions (e.g. polynomial, [19][20]). One of these is the number of parameters, which reduces to three ($\lambda_0$, $L_1$ and $\beta$ ). In fact, thanks to continuity conditions which must apply at the boundary between the two intervals of the domain (i.e. at $|I| = I_{thr}$), low-current linear inductance $L_0$ and the threshold itself can be obtained from the three parameters of the saturation curve. As usual in the presence of magnetic saturation, differential inductance can be defined as

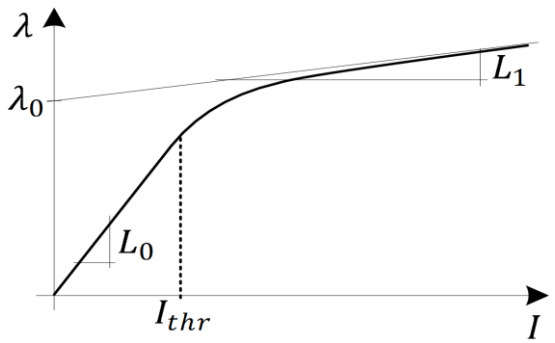

Fig. 1. A typical curve for magnetic saturation model.

$$L_{diff} = \frac{d\lambda}{dI} = L_1 - \frac{\beta}{I^2} \tag{2}$$

while the apparent one will be:

$$L_{app} = \frac{\lambda}{I} = \frac{\lambda_0}{I} + L_1 + \frac{\beta}{I^2} \tag{3}$$

Since the linearity of the flux curve for current values below the threshold, continuity requires apparent and differential inductance in $I_{thr}$ to be equal, i.e.:

$$L_{app}(I_{thr}) = L_{diff}(I_{thr}) \tag{4}$$

$$\frac{\lambda_0}{I_{thr}} + L_1 + \frac{\beta}{I_{thr}^2} = L_1 - \frac{\beta}{I_{thr}^2}$$

which leads to

$$I_{thr} = \frac{-2\beta}{\lambda_0} \tag{5}$$

The linear low-current inductance can be written as the differential inductance calculated in $I_{thr}$

$$L_0 = L_{diff}(I_{thr}) = L_1 - \frac{\lambda_0^2}{4\beta} \tag{6}$$

or as the apparent inductance in the same point

$$L_0 = L_{app}(I_{thr}) = -\frac{\lambda_0^2}{2\beta} + L_1 + \frac{\lambda_0^2}{4\beta} \tag{7}$$

The low number of coefficients considered in this model, and the fact that they appear as multiplying coefficients in the approximating function, allow a simple implementation of least squares identification (Multiple Linear Regression, MLR, [21]) on the drive controller (as it will be shown in the following section). The calculation of inductance (*both apparent and differential*) and flux is a relatively light computational task (e.g. no transcendent functions are involved), which is useful in view of their on-line updating (at each control period) based on the instant value of current.

This model also shows an important advantage over the polynomial functions which are often adopted for the same problem, [20]. In fact, in that case a high-order polynomial usually needs to be considered to achieve a good approximation. This means that a relatively large number of coefficients are implied, and also can result in oscillatory

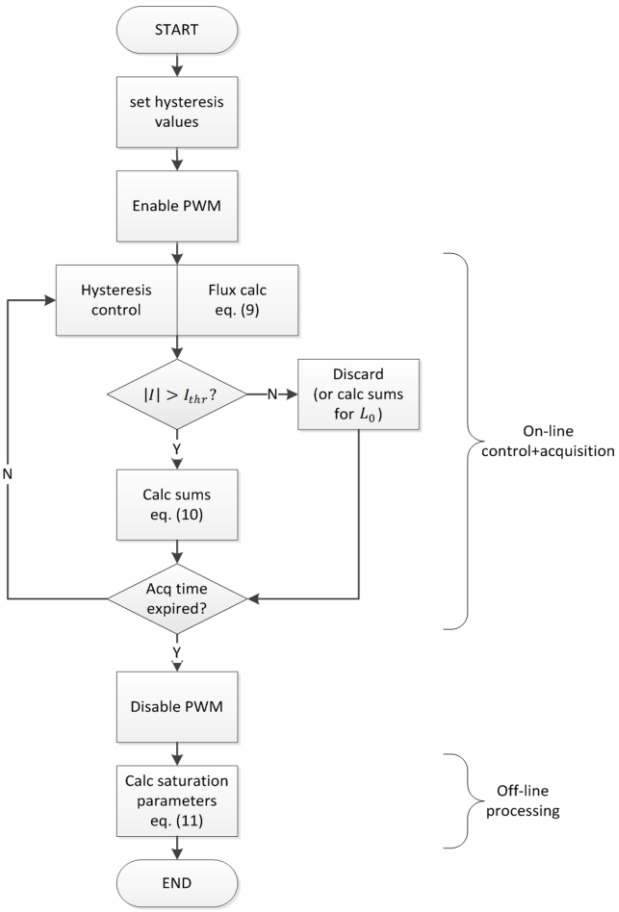


Fig. 2. Flowchart of the proposed identification procedure for one rotor axis.

behavior of the approximating function, which does not allow extrapolation for current values outside the identification range. The physical meaning of the coefficients, in particular $L_1$ and $L_0$ is also an interesting property of this representation for the magnetic saturation.

## III. Self-Commissioning Identification

The self-identification procedure consists in the injection of a voltage signal along each of the two rotor axes, separately (i.e. null voltage on the other axis). To avoid accidental rotation due to low frequency torque components, a proper signal having null average and high frequency content is to be preferred, especially if inertia at the motor shaft is low. The current swing caused by the voltage stimulus must have sufficient amplitude, ideally covering the whole current range of the machine. During the procedure, flux-linkage is estimated for the axis on which the voltage stimulus is applied. At the end of the test, MLR regression to the saturation curve model (1) is performed, based on the acquired current and flux samples.

Let the voltage model of the SynRM in the rotor reference frame be, [22]:

$$\begin{aligned} u_d &= R_s i_d + \frac{d}{dt}\lambda_d - \omega_{me}\lambda_q \\ u_q &= R_s i_q + \frac{d}{dt}\lambda_q + \omega_{me}\lambda_d \end{aligned} \tag{8}$$

where iron core losses have been neglected.

If the stand-still condition is considered (i.e. null electrical speed $\omega_{me}$), no axes coupling is present, thus the flux components $\lambda_{d,q}$ can be estimated by integrating voltage signals on each axes $u_{d,q}$, subtracted by the resistive voltage drop:

$$\lambda_{d,q} = \int \left(u_{d,q} - R_s i_{d,q}\right)\, dt \tag{9}$$

In the actual implementation, integration is performed according to the forward Euler discretization.

If the identification test for either $d$ or $q$ axis is considered, at each time sample $k$ (i.e. in real-time) the following cumulative-sum terms are updated if measured current is larger (in absolute value) than the threshold $I_{thr}$:

$$\begin{matrix} \sum_{k=1}^{n}\lambda_k & \sum_{k=1}^{n} i_k & \sum_{k=1}^{n}\lambda_k i_k \\ \sum_{k=1}^{n} i_k^2 & \sum_{k=1}^{n}\frac{1}{i_k} & \sum_{k=1}^{n}\frac{1}{i_k^2} \quad \sum_{k=1}^{n}\frac{\lambda_k}{i_k} \end{matrix} \tag{10}$$

based on the current and estimated flux samples $i_k$ and $\lambda_k$.

As it will be shown in Appendix, after completion of the procedure, i.e. after $n$ samples have been processed, the quantities just introduced allow to calculate the MLR expression

$$\hat{p} = (x^T x)^{-1}\, x^T y \tag{11}$$

where

$$x = \begin{bmatrix} sign(i_1) & i_1 & \frac{1}{i_1} \\ \dots & \dots & \dots \\ sign(i_n) & i_n & \frac{1}{i_n} \end{bmatrix}, \quad y = \begin{bmatrix} \lambda_1 \\ \dots \\ \lambda_n \end{bmatrix}, \quad \hat{p} = \begin{bmatrix} \hat{\lambda}_0 \\ \hat{L}_1 \\ \hat{\beta} \end{bmatrix} \tag{12}$$

The vector $\hat{p}$ contains the least-squares estimates of the flux model parameters (1) for the high-current case, i.e. $\hat{\lambda}_0$ , $\hat{L}_1$ and $\hat{\beta}$. It is worth noticing that this method avoids the storage of all current and flux samples for post-processing, since it only requires the on-line calculation and storage of the seven variables listed in (10), leading to very limited memory usage and computational effort. An initial guess on the threshold $I_{thr}$, which separates linear and saturation range, is used to start the procedure, but its value is not crucial to the accuracy of results.

As already mentioned, the voltage signal must be chosen so the resulting current samples cover a certain span (usually up to the nominal current), having a sufficient number of points, possibly equally distributed within the desired range. The requirement of null average means that a symmetric signal with respect to zero is a good candidate. To avoid basing the choice of the voltage stimulus waveform on preliminary knowledge about machine inductance, an hysteresis current controller has been adopted, which switches output voltage between two symmetrical (positive and negative) fixed voltage values, based on the comparison of current to two thresholds, set at the maximum and minimum values of the desired current range. The null current average requirement is achieved by setting the current thresholds symmetrically with respect to zero.

Fig. 3. SynRMs adopted in the experimental tests:
industrial drive and motor #1 (top), motor #2 and test-rig (bottom).

From the controller point of view, the identification procedure can be seen as in the flowchart in Fig. 2. Once PWM is enabled, current will swing between the two hysteresis thresholds, while current and voltage samples are acquired. At each sample, flux integration is updated and, if measured current is not within the linear range delimited by $\pm I_{thr}$, the terms to be used for Multiple Linear Regression (10) are updated, too. After the expiration of the desired test length, control is disabled and the actual flux curve parameters are calculated. The samples corresponding to low-current values (i.e. in the non-saturated range) can be exploited to obtain an estimation of the non-saturated inductance $L_0$, by applying straight-line regression. This can be useful for determining the saturation threshold $I_{thr}$ and for a final checking on the correctness of MLR identification, e.g. verifying if the estimated low-current inductance $\hat{L}_0$, determined by means of MLR (according to (6) or (7)), is sufficiently close to the value found by straight-line regression applied to the low-current samples.

As it is clear from its description, the identification method strongly relies on flux-linkage estimation (9). This means that a sufficiently accurate knowledge of the phase resistance value $R_s$ and compensation of the inverter distortion (e.g. due to dead-time) is required, so that reference values $u^*_{d,q}$ can be used to replace voltage measurements $u_{d,q}$. In order to fulfil this condition, a technique for the automatic identification of distortion voltage and resistance at stand-still (such as the one discussed in a very recent paper, [23]) can be applied. In general, the effect that inaccuracy in current measurement, resistance value or dead-time compensation cause on flux estimation can be mitigated by choosing a high test voltage and a proper acquisition time duration to be applied. This choice is indeed a trade-off between noise suppression and other contrasting factors. In fact, high-frequency noise rejection, which is achieved thanks to the averaging effect of MLR, improves with the increasing number of acquired samples. On the other hand, the effect of measurement offset (both current and voltage) typically causes drift of the flux vs. current curve due to integration (9), whose effect gets worse with increasing time. Larger acquisition window length and offset also increase the possibility of a rotor movement, especially in the case the technique is applied to IPM motors, as it will be discussed in the following.

Since identification is based on the rotor synchronous reference frame, it also requires knowledge of the rotor position for Park transformations. Rotor angle information is actually available only in the case a position sensor is present and has been already phased. This should not be taken for granted, considering that the procedure is typically included in a stand-still self-commissioning sequence. However, phasing can be easily achieved by adopting an initial position detection method (e.g. based on high-frequency or pulsed voltage injection, [10]) or, in the SynRM case, by means of DC current alignment (which can involve a limited rotation). Moreover, since the proposed identification procedure requires the rotor to remain almost still during the test, which is achieved by a proper choice of the voltage signal, *position actually needs to be known only before the test*. This means that, by using one of the initial position detection techniques just mentioned, the method can be adopted even in the absence of a position sensor (i.e. in a sensorless drive), which represents a great advantage with respect to other state-of-the-art techniques.

As already mentioned, while in a SynRM the produced torque is theoretically null during identification, this is no more true if extension of the method to the case of Interior Permanent Magnet Synchronous Motors (IPMSM) is considered. In this case, torque is produced when the test signal is applied to the $q$-axis, due to the presence of the permanent magnet. However, if the current has null (or negligible) mean, and its oscillation frequency is sufficiently high with respect to the mechanical pole frequency, rotor movement is very limited. In practical cases, probably thanks to stiction, most motors can be tested with the proposed method, at least up to the motor rated current. Moreover, often the application load is connected to the motor shaft (which is typically the condition in which stand-still identification is mostly needed), making rotor movement even more unlikely to happen.

If a position sensor is available, identification accepts also small accelerations of the rotor, until speed remains low, i.e. rotational voltage components are negligible with respect to the derivative ones:

$$\omega_{me}\lambda_{d,q} \ll \frac{d}{dt}\lambda_{dq} \tag{13}$$

## IV. Experimental Results

The proposed identification algorithm has been implemented using a Gefran ADL200 commercial drive with

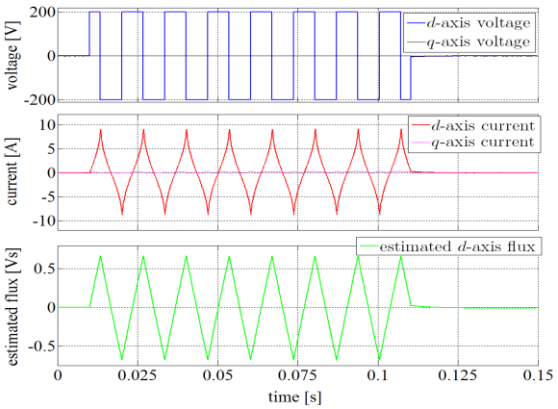


(a) $d$-axis flux identification

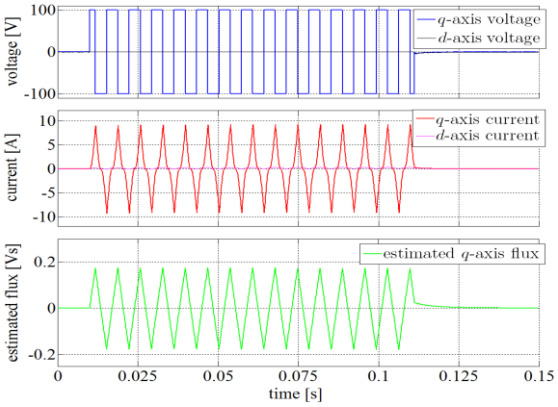


(b) $q$-axis flux identification

Fig. 4. Signal sequence adopted for identification of flux curves.

modified software. Its effectiveness has been verified on two SynRMs (motor #1 and #2) and an IPMSM (motor #3), all of the transverse laminated type. Pictures of the drive and both the reluctance machines are shown in Fig. 3, while the rated parameters of all considered machines are reported in Table I. The drive, which is rated 5.5 kW power, is intended for 400 $V_{RMS}$ three-phase grid supply (with diode rectifier). Controller sampling and update, together with PWM, run at 10 kHz. Fig. 3 also shows the test-rig that has been used to run a high-accuracy technique (i.e. in rotation under load, [15]) for the identification of the considered motors. The results of these tests have been taken as reference for the evaluation of the performance of the proposed algorithms.

Experimental measurements in Fig. 4(a) and (b) show two examples of test signal sequence, which correspond to the identification of direct and quadrature axis flux characteristics of a SynRM (motor #1), respectively. The traces data consist of the values of control variables, which have been downloaded from the drive controller to a personal computer by means of a serial connection. In both cases, the test length is about 100 ms, which corresponds to 1000 time samples. Hysteresis controller output voltage is ±200 V (peak phase voltage) for the $d$-axis and ±100 V for the $q$-axis (since the second is expected to exhibit lower inductance, a reduced voltage has been chosen). The top diagram shows injected voltage, while the middle plot reports both direct and quadrature currents and the bottom one shows the estimated flux-linkage (on the $d$ or $q$-axis, depending on which one is being tested).

As it can be seen, during the injection procedure the axis which is not under identification is kept at null voltage, resulting in a very small current (less than 0.4 A peak). Experiments have shown that this undesired current signal can be reduced (by about one half), by actively controlling current to zero, even with a regulator set for relatively poor dynamics. Although ideally null torque is generated during the test procedure, the contribution of spurious current on the axis not being tested and possible error on the initial position angle could result in rotation, which would be detrimental for the results. In order to evaluate this aspect, Fig. 5 shows the position and speed measurements related to the same kind of test reported in Fig. 4. In both cases, the peak to peak position displacement is less than 1 el. degree and peak speed is below 5 rpm (i.e. less than 0.2% of the nominal speed).

A number of tests have been carried out during the development of this procedure on different motors rated between 1 and 4 kW. Their results suggest that stimulus parameters similar to those adopted in this case, i.e. voltage values between 50 and 200 V and acquisition window durations from 50 to 150 ms should be suitable to the identification of most SynRM and IPMSM in the considered power range, as long as there is a good matching to the adopted inverter in terms of rated voltage and current.

In Fig. 6 the results of identification for the three motors listed in Table I are reported in the form of flux vs. current diagrams for both the $d$ and $q$ axes. The upper and middle plots refer to SynRM machines (motor #1 and #2), while the bottom one refers to an IPMSM machine (motor #3). The stand-still

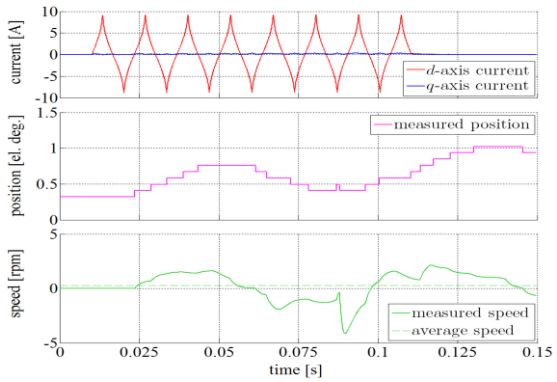


(a) $d$-axis flux identification

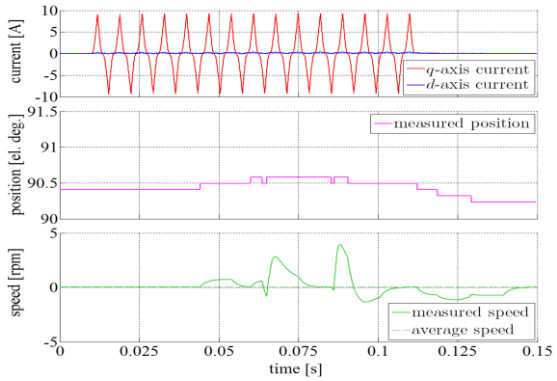


(b) $q$-axis flux identification

Fig. 5. Identification of flux curves: currents vs. mechanical rotation.

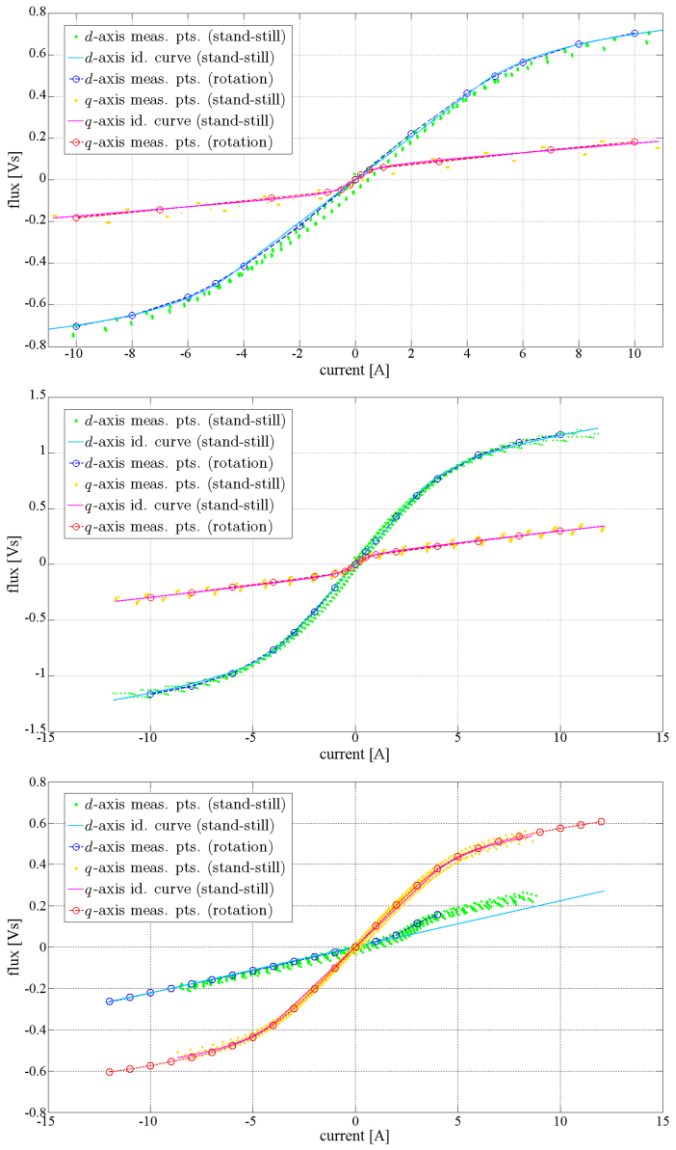


Fig. 6. Identified magnetization curves
(motor #1: top, motor #2: middle, motor #3 bottom).

procedure samples are represented by small dots, while the magnetization curves resulting from the proposed method are drawn as continuous lines. The round markers are obtained by rotational identification. One can notice the good agreement between the stand-still and rotational identification results, which states the accuracy of the proposed technique. In all of the three cases the procedure did not involve using the position signal from the encoder, in order to demonstrate this possibility. High frequency injection techniques were used for the identification of the initial position.

It is worth mentioning that for the IPMSM motor case, it is only possible to identify the inductive component of the $d$-axis, since the permanent magnet component has no electric effect when mechanical speed is zero. In order to allow comparison of the stand-still identification to the reference curve, results of the rotational identification for the direct-axis have been shifted down by subtracting the permanent magnet flux-linkage magnitude value, i.e. the flux measured at $I_d = 0$, $I_q = 0$. Moreover, as it can be seen, the direct-axis curve shows the typical trend related to the saturation of rotor ribs, for positive current values, i.e. flux suddenly increases, until saturation is reached. The asymmetry of this effect (due to the permanent magnet field) makes it difficult to achieve a good fitting using the proposed saturation model. However, since the IPMSM motor will mainly be controlled with $I_d < 0$ (for MTPA), accurate identification in this range has been obtained by approximating the curve to a straight-line (i.e. constant inductance), only considering the negative current samples.

Looking more in detail at the sample points acquired during the stand-still procedure, it appears as if a magnetic hysteresis effect was present. Analysis of the original voltage-current sampled data has shown that voltage integration at the discontinuity points (which are commanded by hysteresis) is critical due to the voltage actuation delay introduced by PWM.

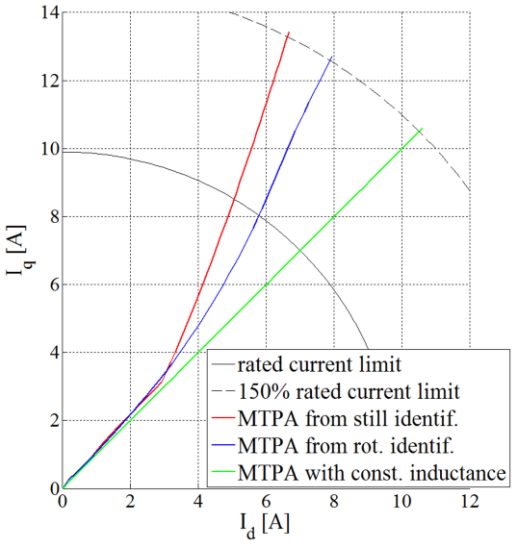


(a) MTPA trajectory in the $I_d I_q$ plane

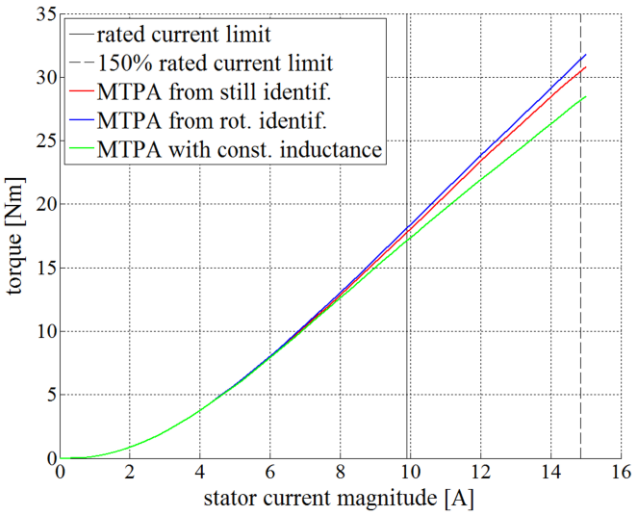


(b) torque vs. current vector magnitude in MTPA

Fig. 7. MTPA loci for motor #2, according to identified flux maps: based on proposed stand-still identification (red), based on rotational identification (blue) and with constant inductances (green).

This effect is however not detrimental to the MLR identification.

As it can be seen especially in the top diagram of Fig. 6, the technique also shows a good robustness to DC offset, which is visible looking at the acquired samples (they are in fact not exactly centered vertically). The DC component is effectively rejected by MLR identification, thanks to the almost symmetrical distribution of the measured current values with respect to zero.

In order to evaluate one of the effects of magnetic motor map accuracy, the Maximum Torque Per Ampere condition has been calculated based on different sets of identification data. The blue curves represented in Fig. 7, related to motor #2, have been obtained from interpolation of flux measurements performed under rotation [15], based on a $I_d I_q$ grid for currents up to 150% of the rated value. The acquisition system accuracy was previously verified by means of combined torque and flux measurements. The results also show the relatively small effect of cross saturation on torque production, at least for this particular motor. In Fig. 7(a), it can be seen that, in the medium to high current range, the trajectory calculated using the stand-still identified flux curves (red) differs from the reference one (blue) which results from rotational identification. In Fig. 7(b) the actual torque calculated for different MTPA loci is related to the corresponding vector current magnitude. When the MTPA locus based on constant inductances (i.e. the green line at 45° angle in Fig. 7(a) is adopted (green curve), the available torque is reduced by an important factor, which is about 6% at the rated current, and reaches 10% at 150% overload. In the same current conditions, the torque reduction for the MTPA trajectory based on the proposed identification is about 2% and 3%, respectively.

The feasibility of implementation on standard controllers has been verified by evaluating the computational cost of the identification algorithm. Flux estimation update (voltage integration, (9)) and accumulation of values for MLR (10) account for 9 sums, 6 multiplications, 3 divisions and 3 signs or absolute value calculation. A time measurement on a typical microcontroller running at 90 MHz has shown that the execution time is about 2.4 µs. The remaining on-line operations are mainly those related to hysteresis current control, which is expected to take approximately the same execution time as typical linear current regulation. A typical Field Oriented Control update routine for a SynRM or IPMSM drive, which usually comprises also speed control, MTPA calculation and other operations such as flux-weakening and checking of limits, must be executed within the PWM and sampling period (typically in the order of 100 µs). Since these operations are not required during identification, it can be concluded that any microcontroller on which SynRM or IPMSM FOC can be implemented is suitable to run the online part of the proposed method. The off-line calculation task consists of 19 sums, 40 multiplications and 1 division, which are performed in about 22.8 µs on the processor considered above. Although its duration can represent a considerable portion of the control period, this task is intended to be run while the drive is not controlled, i.e. when PWM is disabled, so execution time is not crucial.

## V. Full Flux Maps Including Cross-Saturation

If a SynRM is stimulated according to the proposed technique (current hysteresis control) on both axes *simultaneously*, an almost random $dq$ current pattern can be obtained, aiming at exploring the whole current range of the machine. In this case computer post-elaboration was applied on the actual data sampled from the drive controller, since the double identification of both $d$ and $q$ axes was to be performed simultaneously, while the normal implementation considers only one axis at a time.

In order to characterize the whole flux map, for each of the two axes a certain number of different curves is considered, corresponding to different ranges ("slices") of current on the opposite axis. The identification approach exploits the symmetry of the map. It is then repeated for every "slice" (considering the samples that fall within that range), and the curve is assigned to the center of the "slice".

For example, considering the $q$-axis flux map, the $d$-axis current range is divided into a certain number of ranges (“slices”), depending on the desired resolution. Since both d and q axis currents are varying, the current and flux samples corresponding to d axis currents falling within each “slice” will be considered separately. In the end, each slice will result in one curve and thus one set of estimated parameters. A narrower “slice” width means a finer resolution, but also results in a lower number of samples corresponding to each slice (which may become insufficient for the purpose of identification).

An example of the results of this modified procedure is reported in Fig. 8. The direct and quadrature-axis flux map, obtained by means of rotational measurements, are shown for reference as colored surfaces. In both cases, the black spheres represent samples acquired during the stand-still procedure, while the magenta lines are the corresponding identified saturation curves. Each line shows the saturation curve for a 2 A-wide range around a certain current value on the reciprocal axis, and is obtained from points lying in that range. It can be seen that both the sample points and the identified functions are close to the reference surface. Linear interpolation and extrapolation can be applied in order to obtain flux map values over the whole range.

Also in this case, the position measurement from the encoder was not exploited, after a preliminary check stated that very little rotation occurred during the application of the stimulus voltage. However, during the execution of this kind of test, even for a reluctance machine, torque is of course generated. The considerations already done for the IPMSM case also hold in this case, i.e. in most cases rotor movement will be very limited. In order to demonstrate this aspect, the test has been performed on motor #1, which is characterized by very low friction and lower inertia with respect to motor #2 (see approximated inertia values in Table I). Also in this case no external load was connected to the motor shaft. Fig. 9 shows that the resulting displacement was limited to less than 5 electrical degrees peak to peak, while peak speed was less than 19 rpm, i.e. about 0.6% of the nominal value. Considering that the average value of speed during the test was almost null, the influence of speed on the flux computation is negligible. It is also worth noticing that the imposed current swing is up to the

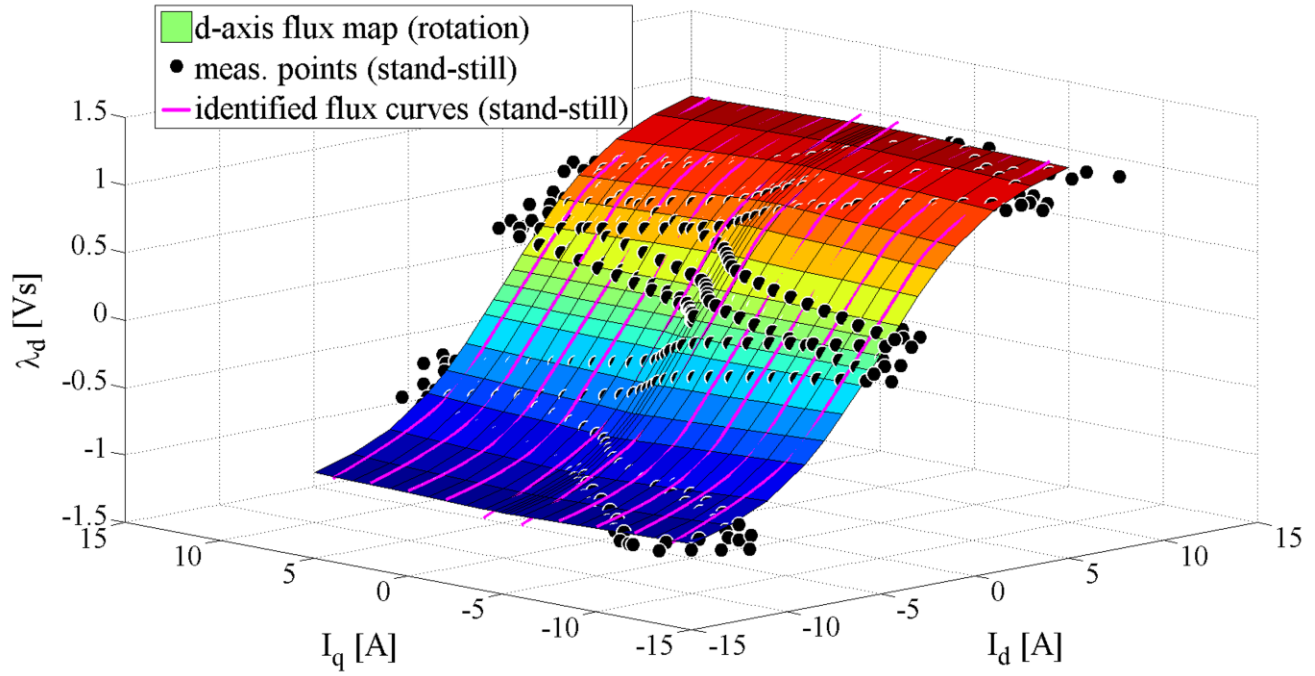


(a) direct-axis

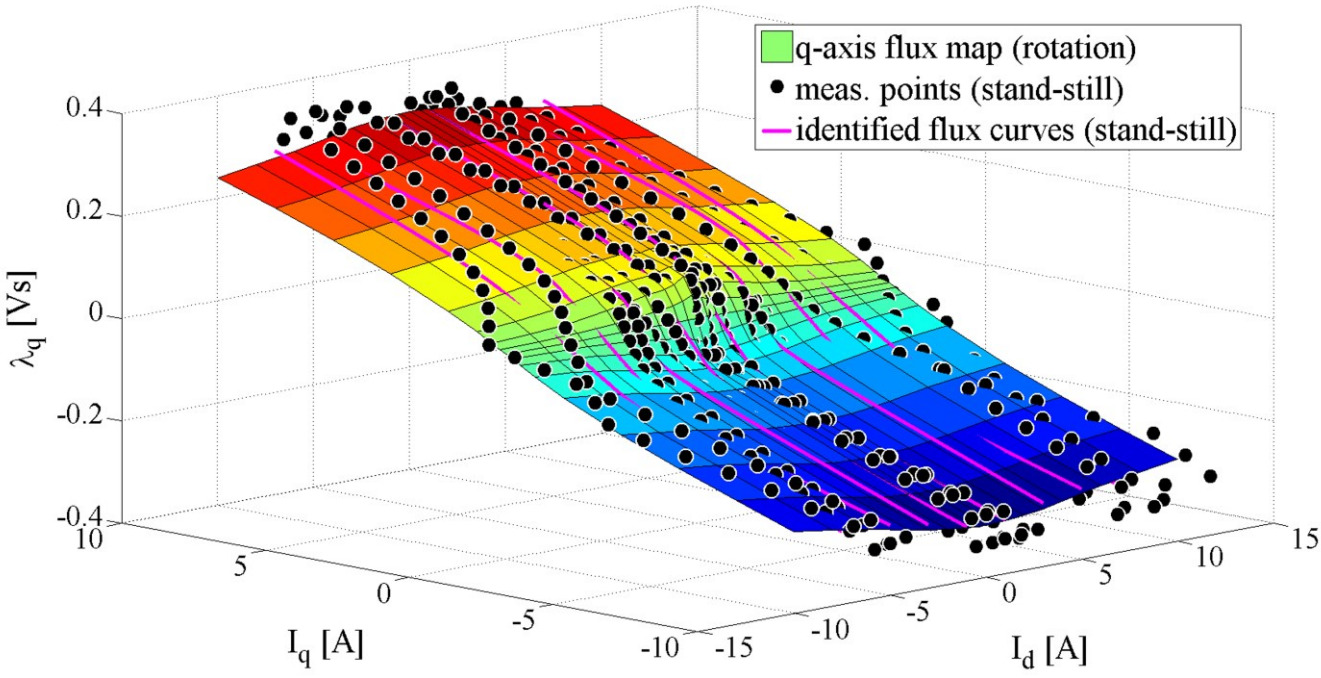


(b) quadrature-axis

Fig. 8. Full flux map exploration at stand-still vs. flux map from rotational tests (motor #2).

nominal current on both axes, thus during the test the current vector magnitude reaches values well beyond the rated current. A narrower range (e.g. up to the peak rated current divided by $\sqrt{2}$, on both axes) may be sufficient in many cases, and would result in reduced mechanical oscillations. As already pointed out, the use of a position measurement for axes transformation would allow to perform the test even if a larger rotation was developed.

## VI. Conclusions

In this paper a self-commissioning identification algorithm for Synchronous Reluctance Motors has been presented, which allows to estimate and describe the direct- and quadrature-axis flux vs. current characteristics, including saturation. A convenient flux saturation approximating function has been introduced, together with an efficient parameters

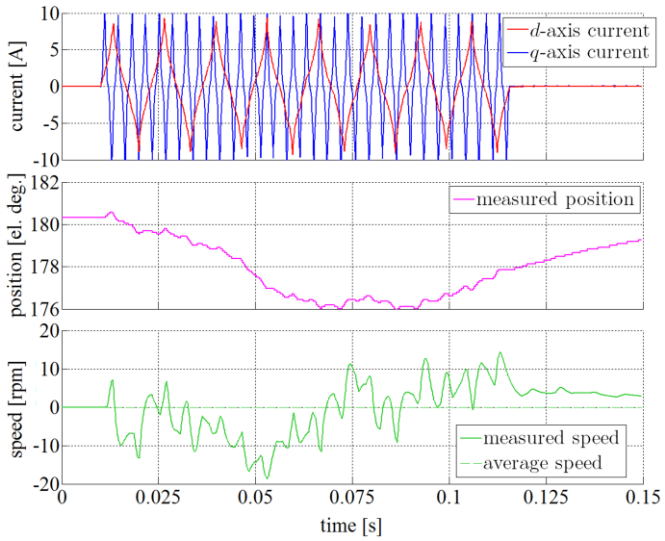


Fig. 9. Signal sequence adopted for identification of flux surfaces.

self-identification procedure. The model for saturated flux curves (which has general validity, and can be applied to different flux measurement methods, too) uses only three parameters and results in an accurate fitting of the actual flux curves, by using Multiple Linear Regression.

The self-identification procedure is very simple and is performed at stand-still by injecting a proper voltage signal, without the need for any prior knowledge of the motor magnetic parameters. Experimental results based on a commercial drive and two SynRM machines has been reported. The comparison to flux measurements obtained at steady-state during rotation shows a very good agreement and prove the effectiveness of the proposal.

Implementation issues, such as the computational effort and commissioning procedure duration has been discussed. Memory usage and computational resources requirements are relatively low, and it is expected that the technique can be applied using any controller suitable to FOC implementation. The range of application of the method is widened by the possibility to perform identification without the use of a position measurement (i.e. in a sensorless drive), which represents an interesting advantage.

Extensions of the technique to the evaluation of the whole flux map of the machine (including cross-saturation effects) and to the case of IPM motors have been demonstrated with success, even if some aspects have to be further investigated and will be the topic of future research.

## APPENDIX

Considering the matrix terms defined in (12), which comprise the sample values $i_k$ and $\lambda_k$, the practical calculation of $\hat{p}$ in equation (11) by means of the terms defined in (10) can be obtained by the following steps. Hereafter, for space and readability reasons, the symbol $\sum$ substitutes $\sum_{k=1}^{n}$.

The first product can be expanded as

$$x^T x = \begin{bmatrix} \sum[\text{sign}(i_k)]^2 & \sum[i_k\ \text{sign}(i_k)] & \sum\left[\frac{1}{i_k}\ \text{sign}(i_k)\right] \\ \sum[i_k\ \text{sign}(i_k)] & \sum i_k^2 & \sum\left(\frac{1}{i_k}\ i_k\right) \\ \sum\left[\frac{1}{i_k}\ \text{sign}(i_k)\right] & \sum\left(\frac{1}{i_k}\ i_k\right) & \sum\frac{1}{i_k^2} \end{bmatrix} \tag{14}$$

and simplified to

$$x^T x = \begin{bmatrix} n & \sum|i_k| & \sum\frac{1}{|i_k|} \\ \sum|i_k| & \sum i_k^2 & n \\ \sum\frac{1}{|i_k|} & n & \sum\frac{1}{i_k^2} \end{bmatrix} \tag{15}$$

Its inverse can be written as (16). The final expression of (11) becomes (17), where the denominator is

$$\begin{aligned} \det(x^T x) = {} & n \cdot \sum\frac{1}{i_k^2} \cdot \sum i_k^2 + 2n \cdot \sum\frac{1}{|i_k|} \cdot \sum|i_k| \\ & - \sum i_k^2 \cdot \left(\sum\frac{1}{|i_k|}\right)^2 - n^3 - \sum\frac{1}{i_k^2} \\ & \cdot \left(\sum|i_k|\right)^2 \end{aligned} \tag{18}$$

It can be highlighted that all of the terms in (17) and (18) depend on cumulative sums (10) and on the number of considered samples $n$.

$$(x^T x)^{-1} = \frac{\begin{bmatrix} \sum i_k^2 \cdot \sum\frac{1}{i_k^2} - n^2 & -\sum|i_k| \cdot \sum\frac{1}{i_k^2} + n \cdot \sum\frac{1}{|i_k|} & \sum|i_k| \cdot n - \sum i_k^2 \cdot \sum\frac{1}{|i_k|} \\ -\sum|i_k| \cdot \sum\frac{1}{i_k^2} + n \cdot \sum\frac{1}{|i_k|} & n \cdot \sum\frac{1}{i_k^2} - \left(\sum\frac{1}{|i_k|}\right)^2 & -n^2 + \sum|i_k| \cdot \sum\frac{1}{|i_k|} \\ \sum|i_k| \cdot n - \sum i_k^2 \cdot \sum\frac{1}{|i_k|} & -n^2 + \sum|i_k| \cdot \sum\frac{1}{|i_k|} & n \cdot \sum i_k^2 - \left(\sum\frac{1}{|i_k|}\right)^2 \end{bmatrix}}{\det(x^T x)} \tag{16}$$

$$\hat{\beta} = \frac{\begin{bmatrix} \left(\sum i_k^2 \cdot \sum\frac{1}{i_k^2} - n^2\right) \cdot \sum[\text{sign}(i_k) \cdot \lambda_k] + \left(-\sum|i_k| \cdot \sum\frac{1}{i_k^2} + n \cdot \sum\frac{1}{|i_k|}\right) \cdot \sum\lambda_k i_k + \sum|i_k| \cdot n - \sum i_k^2 \cdot \sum\frac{1}{|i_k|} \cdot \sum\frac{\lambda_k}{i_k} \\ \left(-\sum|i_k| \cdot \sum\frac{1}{i_k^2} + n \cdot \sum\frac{1}{|i_k|}\right) \cdot \sum[\text{sign}(i_k) \cdot \lambda_k] + \left[n \cdot \sum\frac{1}{i_k^2} - \left(\sum\frac{1}{|i_k|}\right)^2\right] \cdot \sum\lambda_k i_k + \left(-n^2 + \sum|i_k| \cdot \sum\frac{1}{|i_k|}\right) \cdot \sum\frac{\lambda_k}{i_k} \\ \left(\sum|i_k| \cdot n - \sum i_k^2 \cdot \sum\frac{1}{|i_k|}\right) \cdot \sum[\text{sign}(i_k) \cdot \lambda_k] + \left(-n^2 + \sum|i_k| \cdot \sum\frac{1}{|i_k|}\right) \cdot \sum_{i=1}^{n}(i_k \cdot \lambda_k) + \left[n \cdot \sum i_k^2 - \left(\sum\frac{1}{|i_k|}\right)^2\right] \cdot \sum\frac{\lambda_k}{i_k} \end{bmatrix}}{\det(x^T x)} \tag{17}$$

## ACKNOWLEDGEMENTS

This work has been supported by Gefran s.p.a.. The authors wish to thank prof. Gianmario Pellegrino of the Politecnico di Torino for providing one of the test machines.

TABLE I. RATED PARAMETERS OF ADOPTED SYNRMS AND IPMSM

| **Parameter** | **Motor #1** | **Motor #2** | **Motor #3** |
|---|---|---|---|
| Motor type | SynRM | SynRM | IPMSM |
| Power, [kW] | 2.2 | 2.8 | 2.2 |
| Torque, [Nm] | 7 | 18 | 7 |
| Speed, [rpm] | 3000 | 1500 | 3000 |
| Voltage, [$V_{RMS}$, phase-phase] | 360 | 400 | 330 |
| Current, [$A_{RMS}$] | 5.6 | 7 | 4.2 |
| Pole pairs | 2 | 2 | 2 |
| $d$-axis inductance, [mH] | 90 | 212 | 22 |
| $q$-axis inductance, [mH] | 11 | 29 | 95 |
| PM flux magnitude, [Vs] | - | - | 0.237 |
| Moment of inertia, [kg·m$^2$] | 0.004 | 0.0025 | 0.001 |

## REFERENCES

[1] J. Faucher, M. Lajoie-Mazenc, and A. Chayegani, "Characterization of a Closed-Loop Controlled Current-Fed Reluctance Machine Taking into Account Saturation," *IEEE Transactions on Industry Applications*, vol. IA-15, no.5, pp.482-488, Sept. 1979.

[2] A. Fratta, and A. Vagati, "A Reluctance Motor Drive for High Dynamic Performance Applications," *IEEE Transactions on Industry Applications*, vol. 28, no. 4, July/Aug. 1992.

[3] T. Matsuo, and T. A. Lipo, "Field oriented control of synchronous reluctance machine," in *Proc. of Power Electronics Specialists Conference*, Seattle, WA, June 1993, pp. 425–433.

[4] A. Vagati, "The synchronous reluctance solution: a new alternative in AC drives," in *Proc. of the 20th International Conference on Industrial Electronics, Control and Instrumentation*, vol. 1, no., pp.1-13, 5-9 Sept. 1994.

[5] S. Taghavi, and P. Pillay, "A Sizing Methodology of the Synchronous Reluctance Motor for Traction Applications," *IEEE Journal of Emerging and Selected Topics in Power Electronics*, pp. 329-340, June 2014.

[6] S. Taghavi, and P. Pillay, "Mechanically Robust Rotor with Transverse-Laminations for a Wide Speed Range Synchronous Reluctance Traction Motor," *IEEE Tran. on Industry Applications*, vol. 51, no. 6, Nov./Dec. 2015

[7] M. Morandin, E. Fornasiero, N. Bianchi, and S. Bolognani, "Robust Integrated Starter/Alternator Drive Adopting a Synchronous Reluctance Machine for Automotive Applications," *Proc. of IEEE Transportation Electrification Conference and Expo*, 2014.

[8] M. Ferrari, N. Bianchi, A. Doria and E. Fornasiero, "Design of Synchronous Reluctance Motor for Hybrid Electric Vehicles," *IEEE Trans. on Industry Applications*, vol. 51, no. 4, pp. 3030-3040, July-Aug. 2015.

[9] T. Tuovinen, and M. Hinkkanen, "Signal-Injection-Assisted Full-Order Observer With Parameter Adaptation for Synchronous Reluctance Motor Drives, " *IEEE Trans. on Industry Applications*, vol. 50, no. 5, pp. 3392-3402, Sept.-Oct. 2014.

[10] F.J.W. Barnard, W.T. Villet, and M.J. Kamper, "Hybrid Active-Flux and Arbitrary Injection Position Sensorless Control of Reluctance Synchronous Machines," *IEEE Trans. on Industry Applications*, early access paper, 2015.

[11] M.J. Kamper, "Effect of rotor dimensions and cross magnetisation on Ld and Lq inductances of reluctance synchronous machine with cageless flux barrier rotor," *IEE Proceedings Electric Power Applications*, vol.141, no.4, pp.213-220, Jul 1994.

[12] A. Vagati, M. Pastorelli, F. Scapino, and G. Franceschini, "Impact of cross saturation in synchronous reluctance motors of the transverse-laminated type," *IEEE Transactions on Industry Applications*, vol. 36, no. 4, pp. 1039-1046, July-Aug. 2000.

[13] Y. Li, Z.Q. Zhu, D. Howe, and C.M. Bingham, "Modeling of Cross-Coupling Magnetic Saturation in Signal-Injection-Based Sensorless Control of Permanent-Magnet Brushless AC Motors," *IEEE Transactions on Magnetics*, vol.43, no.6, pp.2552-2554, June 2007.

[14] S. Kuehl, and R.M. Kennel, "Measuring Magnetic Characteristics of Synchronous Machines by Applying Position Estimation Techniques," *IEEE Transactions on Industry Applications*, pp. 3816-3824, vol. 50, no. 6, Nov.-Dec. 2014.

[15] E. Armando, R. I. Bojoi, P. Guglielmi, G. Pellegrino, and M. Pastorelli, "Experimental Identification of the Magnetic Model of Synchronous Machines," *IEEE Transactions on Industry Applications*, vol. 49, no. 5, pp. 2116–2125, Sept. 2013.

[16] G. Pellegrino, B. Boazzo, and T.M. Jahns, "Magnetic Model Self-Identification for PM Synchronous Machine Drives," *IEEE Transactions on Industry Applications*, vol. 51, no. 3, pp. 2246-2254, May-June 2015.

[17] S. A. Odhano, P. Giangrande, R. I. Bojoi, and C. Gerada, "Self-Commissioning of Interior Permanent-Magnet Synchronous Motor Drives With High-Frequency Current Injection", *IEEE Transactions on Industry Applications*, vol. 50, no. 5, pp. 3295–3303, Sept. 2014.

[18] S.A. Odhano, R. Bojoi, S.G. Rosu, and A. Tenconi, "Identification of the magnetic model of permanent magnet synchronous machines using DC-biased low frequency AC signal injection," *IEEE Transactions on Industry Applications*, vol. 51, no. 4, pp. 3208-3215, July-Aug. 2015.

[19] T. Lubin, H. Razik, and A. Rezzoug, "Magnetic Saturation Effects on the Control of a Synchronous Reluctance Machine," IEEE Transactions on Energy Conversion, vol. 17, no. 3, Sept. 2002.

[20] M. Seilmeier, and B. Piepenbreier, "Identification of steady-state inductances of PMSM using polynomial representations of the flux surfaces," *Proc. of the 39th Annual Conference of the IEEE Industrial Electronics Society*, pp. 2899-2904, 10-13 Nov. 2013.

[21] G. H. Golub, and C. F. Van Loan, Matrix Computations, 3rd Edition, Baltimore, The Johns Hopkins University Press, 1996.

[22] R. H. Park, "Two-reaction theory of synchronous machines generalized method of analysis-part I", Transactions of the American Institute of Electrical Engineers, vol. 48, n. 3, pp. 716–727, July 1929.

[23] N. Bedetti, S. Calligaro, and R. Petrella, "Self-commissioning of inverter dead-time compensation by multiple linear regression based on a physical model," *IEEE Transactions on Industry Applications*, vol. 51, no. 5, pp. 3954-3964, Sept.-Oct. 2015.